Pseudospin symmetry in Zr and Sn isotopes from the proton drip line to the neutron drip line

J. Meng,[1,2,3] K. Sugawara-Tanabe,[2,4] S. Yamaji,[2] and A. Arima[2]
[1]*Department of Technical Physics, Peking University, Beijing 100871, People's Republic of China*
[2]*The Institute of Physical and Chemical Research (RIKEN), Hirosawa 2-1, Wako-shi, Saitama, 351-0198 Japan*
[3]*Institute of Modern Physics, Chinese Academy of Sciences, Lanzhou 730000, China*
[4]*Otsuma Women's University, Tama, Tokyo 206-8540, Japan*
(Received 5 August 1998)

Based on the relativistic continuum Hartree-Bogoliubov theory, the pseudospin approximation in exotic nuclei is investigated in Zr and Sn isotopes from the proton drip line to the neutron drip line. The quality of the pseudospin approximation is shown to be connected to the competition between the pseudocentrifugal barrier and the pseudospin orbital potential (PSOP). The PSOP depends on the derivative of the difference between the scalar and vector potentials dV/dr. If $dV/dr=0$, the pseudospin symmetry is exact. The pseudospin symmetry is found to be a good approximation for normal nuclei and to become much better for exotic nuclei with a highly diffuse potential, which have $dV/dr\sim 0$. The energy splitting of the pseudospin partners is smaller for orbitals near the Fermi surface (even in the continuum) than the deeply bound orbitals. The lower components of the Dirac wave functions for the pseudospin partners are very similar and almost equal in magnitude. [S0556-2813(99)00801-8]

PACS number(s): 21.10.Hw, 21.10.Pc, 21.60.Jz, 27.60.+j

I. INTRODUCTION

The concept of pseudospin is based on the experimental observation that single particle orbitals with $j=l+1/2$ and $j=(l+2)-1/2$ lie very close in energy and can therefore be labeled as pseudospin doublets with quantum number $\tilde{n}=n-1$, $\tilde{l}=l-1$, and $\tilde{s}=s=1/2$. This concept was originally found in spherical nuclei 30 years ago [1,2], but later proved to be a good approximation in deformed nuclei as well [3]. It is shown that the pseudospin symmetry remains an important physical concept even in the case of triaxiality [4].

Since the suggestion of pseudospin symmetry, much effort has been made to understand its origin. Apart from the rather formal relabeling of quantum numbers, various proposals for an explicit transformation from the normal scheme to the pseudospin scheme have been made in the last 20 years and several nuclear properties have been investigated in this scheme [5–9]. Based on the single-particle Hamiltonian of the oscillator shell model the origin of pseudospin was proved to be connected to the special ratio in the strength of the spin-orbit and orbit-orbit interactions [10,8] and the unitary operator performing a transformation from normal spin to pseudospin space was discussed [8–12]. However, it was not explained why this special ratio is allowed in nuclei. The relation between the pseudospin symmetry and relativistic mean field (RMF) theory [13] was first noted in Ref. [7], in which Bahri *et al.* found that the RMF explains approximately the strengths of spin-orbit and orbit-orbit interactions in nonrelativistic calculations. In a recent paper Ginocchio took this a step further and revealed that pseudo-orbital angular momentum is nothing but the ''orbital angular momentum'' of the lower component of the Dirac wave function [14]. He also built a connection between the pseudospin symmetry and the equality in magnitude but difference in sign in the scalar and vector potentials [14,15].

To understand to what extent it is broken in real nuclei, some investigation along this line has been done for square well potentials [14] and for spherical solutions of the RMF equations [16]. By relating the pseudospin symmetry back to the Dirac equation through the framework of relativistic continuum Hartree-Bogoliubov (RCHB) theory [18], the pseudospin approximation in real nuclei was shown to be connected to the competition between the pseudocentrifugal barrier (PCB) and the pseudospin orbital potential (PSOP), which is mainly decided by the derivative of the difference between the scalar and vector potentials. This is general for any Dirac spinor system with spherical symmetry. With the scalar and vector potentials derived from a self-consistent relativistic Hartree-Bogoliubov calculation, the pseudospin symmetry and its energy dependence have been discussed in Ref. [17].

Highly unstable nuclei with extreme proton and neutron ratios are now accessible with the help of radioactive nuclear beam facilities. The physics connected to the extreme neutron richness in these nuclei and the low density in the tails of their distributions has attracted more and more attention not only in nuclear physics but also in other fields such as astrophysics [19,20]. New exciting discoveries have been made by exploring hitherto inaccessible regions in the nuclear chart. It is very interesting to investigate the pseudospin symmetry approximation both in normal and exotic nuclei. For this purpose, we will use RCHB theory, which is the extension of the RMF and the Bogoliubov transformation in the coordinate representation, and provides not only a unified description of the mean field and pairing correlation but also the proper description for the continuum and its coupling with the bound state [18,21]. As this theory takes into account the proper isospin dependence of the spin-orbit term, it is able to provide a good description of global experimental data not only for stable nuclei but also for exotic nuclei throughout the nuclear chart [18]. It is very interesting to examine the pseudospin symmetry approximation in exotic

nuclei, in which the mean field potentials are expected to be highly diffuse.

Here we will extend the previous investigation to the case of exotic nuclei. The pseudospin splitting in Zr and Sn isotopes has been studied from the proton drip line to the neutron drip line. The energy splitting of the pseudospin partners and their energy and isospin dependence will be addressed. An outline of the RCHB formalism is briefly reviewed in Sec. II. In Sec. III, the Dirac equation and the formalism leading to the pseudospin symmetry is presented. The energy splitting of the pseudospin partners and its energy dependence are given in Sec. IV. The pseudospin orbital potential, which breaks the pseudospin symmetry, will be studied in Sec. V. In Sec. VI, the wave function of pseudospin partners will be studied. A brief summary is given in the last section.

II. OUTLINE OF RCHB THEORY

RCHB theory is obtained by combining the RMF and the Bogoliubov transformation in the coordinate representation [21], and its detailed formalism and numerical solution can be found in Ref. [18] and references therein. RCHB theory can give a fully self-consistent description of the chain of lithium isotopes [21] ranging from ^{6}Li to ^{11}Li. The halo in ^{11}Li has been successfully reproduced in this self-consistent picture and excellent agreement with recent experimental data is obtained. The contribution from the continuum has been taken into account and proved to be crucial to understand the halo in exotic nuclei. Based on RCHB theory, a new phenomenon, ''giant halo,'' has been predicted. The ''giant halo'' is composed not only of one or two neutrons, as is the case in halos in light *p*-shell nuclei, but also up to six neutrons [22]. The development of skins and halos and their relation to the shell structure are systematically studied with RCHB theory in Ref. [23], where both pairing and blocking effects have been treated self-consistently. Therefore RCHB theory is very suitable for the examination of the pseudospin approximation in exotic nuclei.

The basic ansatz of RMF theory starts from a Lagrangian density by which nucleons are described as Dirac particles interacting via the exchange of various mesons and photons. The mesons considered are the scalar sigma (σ), vector omega (ω), and isovector vector rho ($\vec{\rho}$). The isovector vector rho ($\vec{\rho}$) meson provides the necessary isospin asymmetry. The scalar sigma meson moves in the self-interacting field of cubic and quadratic terms with strengths g_2 and g_3, respectively. The Lagrangian then consists of free baryon and meson parts and the interaction part with minimal coupling, together with the nucleon mass M, and $m_\sigma, g_\sigma, m_\omega, g_\omega, m_\rho, g_\rho$, the masses and coupling constants of the respective mesons:

$$\begin{aligned}\mathcal{L}=&\bar{\psi}(i\not{\partial}-M)\psi+\frac{1}{2}\partial_\mu\sigma\partial^\mu\sigma-U(\sigma)-\frac{1}{4}\Omega_{\mu\nu}\Omega^{\mu\nu}\\&+\frac{1}{2}m_\omega^2\omega_\mu\omega^\mu-\frac{1}{4}\vec{R}_{\mu\nu}\vec{R}^{\mu\nu}+\frac{1}{2}m_\rho^2\vec{\rho}_\mu\vec{\rho}^\mu-\frac{1}{4}F_{\mu\nu}F^{\mu\nu}\\&-g_\sigma\bar{\psi}\sigma\psi-g_\omega\bar{\psi}\not{\omega}\psi-g_\rho\bar{\psi}\not{\vec{\rho}}\vec{\tau}\psi-e\bar{\psi}\not{A}\psi.\end{aligned}\tag{1}$$

The field tensors for the vector mesons are given as

$$\begin{aligned}\Omega^{\mu\nu}&=\partial^\mu\omega^\nu-\partial^\nu\omega^\mu,\\ \vec{R}^{\mu\nu}&=\partial^\mu\vec{\rho}^\nu-\partial^\nu\vec{\rho}^\mu-g^\rho(\vec{\rho}^\mu\times\vec{\rho}^\nu),\\ F^{\mu\nu}&=\partial^\mu\vec{A}^\nu-\partial^\nu\vec{A}^\mu.\end{aligned}\tag{2}$$

For a realistic description of nuclear properties, a nonlinear self-coupling of the scalar mesons turns out to be crucial [24]:

$$U(\sigma)=\frac{1}{2}m_\sigma^2\sigma^2+\frac{g_2}{3}\sigma^3+\frac{g_3}{4}\sigma^4.\tag{3}$$

The classical variation principle gives the following equations of motion:

$$\{\vec{\alpha}\cdot\vec{p}+V_V(\vec{r})+\beta[M+V_S(\vec{r})]\}\psi_i=\epsilon_i\psi_i\tag{4}$$

for the nucleon spinors and

$$\begin{aligned}-\Delta\sigma+U'(\sigma)&=-g_\sigma\rho_s,\\ (-\Delta+m_\omega^2)\omega^\mu&=g_\omega j^\mu(\vec{r}),\\ (-\Delta+m_\rho^2)\vec{\rho}^\mu&=g_\rho\vec{j}^\mu(\vec{r}),\\ -\Delta A_0^\mu(\vec{r})&=ej_p^\mu(\vec{r}),\end{aligned}\tag{5}$$

with $U'(\sigma)=\partial_\sigma U(\sigma)$ and $\Delta=-\partial^\mu\partial_\mu$ for the mesons, where

$$V_V(\vec{r})=g_\omega\not{\omega}+g_\rho\not{\vec{\rho}}\vec{\tau}+\frac{1}{2}e(1-\tau_3)\not{A},\quad V_S(\vec{r})=g_\sigma\sigma(\vec{r})\tag{6}$$

are the vector and scalar potentials, respectively, and the source terms for the mesons are

$$\begin{aligned}\rho_s&=\sum_{i=1}^{A}\bar{\psi}_i\psi_i,\quad j^\mu(\vec{r})=\sum_{i=1}^{A}\bar{\psi}_i\gamma^\mu\psi_i,\\ \vec{j}^\mu(\vec{r})&=\sum_{i=1}^{A}\bar{\psi}_i\gamma^\mu\vec{\tau}\psi_i,\quad j_p^\mu(\vec{r})=\sum_{i=1}^{A}\bar{\psi}_i\gamma^\mu\frac{1-\tau_3}{2}\psi_i,\end{aligned}\tag{7}$$

where the summations are over the valence nucleons only. It should be noted that as usual, the present approach neglects the contribution of negative energy states, i.e., the no-sea approximation, which means that the vacuum is not polarized. The coupled equations (4) and (5) are nonlinear quantum field equations, and their exact solutions are very complicated. Thus the mean field approximation is generally used: i.e., the meson field operators in Eq. (4) are replaced by their expectation values, so that the nucleons move independently in the classical meson fields. The coupled equations are self-consistently solved by iteration.

For spherical nuclei, i.e., systems with rotational symmetry, the potential of the nucleon and the sources of meson fields depend only on the radial coordinate r. The spinor is characterized by the quantum numbers l, j, and m, and the

isospin $t=\pm\frac{1}{2}$ for neutrons and protons, respectively. The other quantum number is denoted by i. The Dirac spinor has the form

$$\psi(\vec{r})=\begin{pmatrix} g \\ f \end{pmatrix}=\begin{pmatrix} \mathrm{i}\dfrac{G_i^{lj}(r)}{r}Y_{jm}^{l}(\theta,\phi) \\ \dfrac{F_i^{lj}(r)}{r}(\vec{\sigma}\cdot\hat{\vec{r}})Y_{jm}^{l}(\theta,\phi) \end{pmatrix}\chi_t(t), \tag{8}$$

where $Y_{jm}^{l}(\theta,\phi)$ are the spinor spherical harmonics and $G_i^{lj}(r)$ and $F_i^{lj}(r)$ are the radial wave function for upper and lower components. They are normalized according to the relation

$$\int_0^\infty dr[|G_i^{lj}(r)|^2+|F_i^{lj}(r)|^2]=1. \tag{9}$$

The radial equation of spinors, Eq. (4), can be reduced as

$$\epsilon_i G_i^{lj}(r)=\left(-\frac{\partial}{\partial r}+\frac{\kappa_i}{r}\right)F_i^{lj}(r)+[M+V_S(r)+V_V(r)]G_i^{lj}(r),$$

$$\epsilon_i F_i^{lj}(r)=\left(+\frac{\partial}{\partial r}+\frac{\kappa_i}{r}\right)G_i^{lj}(r)-[M+V_S(r)-V_V(r)]F_i^{lj}(r), \tag{10}$$

where

$$\kappa=\begin{cases} -(j+1/2) & \text{for } j=l+1/2, \\ +(j+1/2) & \text{for } j=l-1/2. \end{cases}$$

The meson field equations become simply radial Laplace equations of the form

$$\left(-\frac{\partial^2}{\partial r^2}-\frac{2}{r}\frac{\partial}{\partial r}+m_\phi^2\right)\phi=s_\phi(r), \tag{11}$$

where m_ϕ are the meson masses for $\phi=\sigma,\omega,\rho$ and for photons ($m_\phi=0$). The source terms are

$$s_\phi(r)=\begin{cases} -g_\sigma\rho_s-g_2\sigma^2(r)-g_3\sigma^3(r) & \text{for the } \sigma \text{ field}, \\ g_\omega\rho_v & \text{for the } \omega \text{ field}, \\ g_\rho\rho_3(r) & \text{for the } \rho \text{ field}, \\ e\rho_c(r) & \text{for the Coulomb field}, \end{cases} \tag{12}$$

$$4\pi r^2\rho_s(r)=\sum_{i=1}^{A}[|G_i(r)|^2-|F_i(r)|^2],$$

$$4\pi r^2\rho_v(r)=\sum_{i=1}^{A}[|G_i(r)|^2+|F_i(r)|^2],$$

$$4\pi r'^2\rho_3(r)=\sum_{p=1}^{Z}[|G_p(r)|^2+|F_p(r)|^2]-\sum_{n=1}^{N}[|G_n(r)|^2+|F_n(r)|^2],$$

$$4\pi r^2\rho_c(r)=\sum_{p=1}^{Z}[|G_p(r)|^2+|F_p(r)|^2]. \tag{13}$$

The Laplace equation can be solved by using the Green's function:

$$\phi(r)=\int_0^\infty r'^2dr'G_\phi(r,r')s_\phi(r'), \tag{14}$$

where for massive fields

$$G_\phi(r,r')=\frac{1}{2m_\phi}\frac{1}{rr'}(e^{-m_\phi|r-r'|}-e^{-m_\phi|r+r'|}) \tag{15}$$

and for the Coulomb field

$$G_\phi(r,r')=\begin{cases} 1/r & \text{for } r>r', \\ 1/r' & \text{for } r<r'. \end{cases} \tag{16}$$

Equations (10) and (11) could be solved self-consistently in the usual RMF approximation. However, Eq. (10) does not contain the pairing interaction, as the classical meson fields are used in RMF theory. In order to have the pairing interaction, one has to quantize the meson fields, which leads to a Hamiltonian with a two-body interaction. Following the standard procedure of Bogoliubov transformation, a Dirac Hartree-Bogoliubov equation could be derived and then a unified description of the mean field and pairing correlation in nuclei could be achieved. For details, see Ref. [18] and references therein. The RHB equations are as follows:

$$\int d^3r'\begin{pmatrix} h-\lambda & \Delta \\ \Delta & -h+\lambda \end{pmatrix}\begin{pmatrix} \psi_U \\ \psi_V \end{pmatrix}=E\begin{pmatrix} \psi_U \\ \psi_V \end{pmatrix}, \tag{17}$$

where

$$h(\vec{r},\vec{r}')=\{\vec{\alpha}\cdot\vec{p}+V_V(\vec{r})+\beta[M+V_S(\vec{r})]\}\delta(\vec{r},\vec{r}') \tag{18}$$

is the Dirac Hamiltonian and the Fock term has been neglected as is usually done in RMF theory. The pairing potential is

$$\Delta_{kk'}(\vec{r},\vec{r}')=-\int d^3r_1\int d^3r_1' \times\sum_{\tilde{k}\tilde{k}'}V_{kk',\tilde{k}\tilde{k}'}(\vec{r}\vec{r}';\vec{r}_1\vec{r}_1')\kappa_{\tilde{k}\tilde{k}'}(\vec{r}_1,\vec{r}_1'). \tag{19}$$

It is obtained from the one-meson-exchange interaction $V_{kk',\tilde{k}\tilde{k}'}(\vec{r}\vec{r}';\vec{r}_1\vec{r}_1')$ in the pp channel and the pairing tensor $\kappa=V^*U^T$:

$$\kappa_{kk'}(\vec{r},\vec{r}')=\langle|a_ka_{k'}|\rangle=\psi_V^k(\vec{r})^*\psi_U^{k'}(\vec{r})^T. \tag{20}$$

The nuclear density is as follows:

$$\rho(\vec{r},\vec{r}')=\sum_{ilj} g_{ilj}\psi_V^{ilj}(\vec{r})^*\psi_V^{ilj}(\vec{r}'). \tag{21}$$

As in Ref. [18], V used for the pairing potential in Eq. (19) is either a density-dependent two-body force of zero range with interaction strength V_0 and nuclear matter density ρ_0,

$$V(\boldsymbol{r}_1,\boldsymbol{r}_2)=V_0\delta(\boldsymbol{r}_1-\boldsymbol{r}_2)\frac{1}{4}[1-\boldsymbol{\sigma}_1\boldsymbol{\sigma}_2]\left(1-\frac{\rho(r)}{\rho_0}\right), \tag{22}$$

or a Gogny-type finite-range force with the parameters μ_i, W_i, B_i, H_i, and M_i $(i=1,2)$ [25]:

$$V(\boldsymbol{r}_1,\boldsymbol{r}_2)=\sum_{i=1,2} e^{[(\boldsymbol{r}_1-\boldsymbol{r}_2)/\mu_i]^2}(W_i+B_iP^\sigma-H_iP^\tau-M_iP^\sigma P^\tau). \tag{23}$$

A Lagrange multiplier λ is introduced to fix the particle number for the neutron and proton as $N=\mathrm{Tr}\,\rho_n$ and $Z=\mathrm{Tr}\,\rho_p$.

In order to describe both continuum and bound states self-consistently, we use RHB theory in a coordinate representation, i.e., the relativistic continuum Hartree-Bogoliubov theory [18]. It is then applicable to both exotic nuclei and normal nuclei. In Eq. (17), the eigenstates occur in pairs of opposite energies. When spherical symmetry is imposed on the solution of the RCHB equations, the wave function can be written as

$$\psi_U^i=\begin{pmatrix} \mathrm{i}\dfrac{G_U^{ilj}(r)}{r} \\ \dfrac{F_U^{ilj}(r)}{r}(\vec{\sigma}\cdot\hat{\vec{r}}) \end{pmatrix} Y_{jm}^l(\theta,\phi)\chi_t(t),$$

$$\psi_V^i=\begin{pmatrix} \mathrm{i}\dfrac{G_V^{ilj}(r)}{r} \\ \dfrac{F_V^{ilj}(r)}{r}(\vec{\sigma}\cdot\hat{\vec{r}}) \end{pmatrix} Y_{jm}^l(\theta,\phi)\chi_t(t). \tag{24}$$

Using the above equation, Eq. (17) depends only on the radial coordinates and can be expressed as the following integro-differential equations:

$$\frac{dG_U(r)}{dr}+\frac{\kappa}{r}G_U(r)-[E+\lambda-V_V(r)+V_S(r)]F_U(r)+r\int r'dr'\Delta(r,r')F_V(r')=0,$$

$$\frac{dF_U(r)}{dr}-\frac{\kappa}{r}F_U(r)+[E+\lambda-V_V(r)-V_S(r)]G_U(r)+r\int r'dr'\Delta(r,r')G_V(r')=0,$$

$$\frac{dG_V(r)}{dr}+\frac{\kappa}{r}G_V(r)+[E-\lambda+V_V(r)-V_S(r)]F_V(r)+r\int r'dr'\Delta(r,r')F_U(r')=0,$$

$$\frac{dF_V(r)}{dr}-\frac{\kappa}{r}F_V(r)-[E-\lambda+V_V(r)+V_S(r)]G_V(r)+r\int r'dr'\Delta(r,r')G_U(r')=0, \tag{25}$$

where the nucleon mass is included in the scalar potential $V_S(r)$. For the δ force of Eq. (22), Eq. (25) is reduced to normal coupled differential equations and can be solved with the shooting method by Runge-Kutta algorithms. For the case of Gogny force, the coupled integro-differential equations are discretized in space and solved by finite-element methods. The numerical details can be found in Ref. [18]. Now we have to solve Eqs. (25) and (11) self-consistently for the RCHB case. As the calculation with Gogny force is very time-consuming, we solve them only for one case in order to fix the interaction strength for the δ force in Eq. (22).

III. PSEUDOSPIN SYMMETRY

The Dirac equation in RMF theory or in the canonical basis of RCHB theory describes a Dirac spinor with mass M moving in a scalar potential $V_S(\vec{r})$ and a vector potential $V_V(\vec{r})$. With $\epsilon=M+E$, the potential $V=V_V(\vec{r})+V_S(\vec{r})$, which is around -50 MeV, and the effective mass $M^*=M+V_S(\vec{r})$, the relation between the upper and lower components of the wave function can be written as

$$g=\frac{1}{E-V}(\vec{\sigma}\cdot\vec{p})f, \quad f=\frac{1}{E+2M^*-V}(\vec{\sigma}\cdot\vec{p})g. \tag{26}$$

Then the coupled equations are reduced to uncoupled ones for the upper and lower components, respectively. Effectively we get the corresponding Schrödinger equation for both components:

$$(\vec{\sigma}\cdot\vec{p})\frac{1}{E+2M^*-V}(\vec{\sigma}\cdot\vec{p})g=(E-V)g,\quad (\vec{\sigma}\cdot\vec{p})\frac{1}{E-V}(\vec{\sigma}\cdot\vec{p})f=(E+2M^*-V)f. \tag{27}$$

In the spherical case, V depends only on the radius. We choose the phase convention of the vector spherical harmonics as

$$(\vec{\sigma}\cdot\vec{r})Y^l_{jm}=-Y^{l'}_{jm}, \tag{28}$$

where

$$l'=2j-l=\begin{cases} l+1, & j=l+1/2, \\ l-1, & j=l-1/2. \end{cases} \tag{29}$$

Here l' is nothing but the pseudo-orbital angular momentum $\tilde{l}$. After some tedious procedures, one gets the radial equation for the lower and upper components, respectively:

$$\left[\frac{d^2}{dr^2}+\frac{1}{E-V}\frac{dV}{dr}\frac{d}{dr}\right]F^{lj}_i(r)+\left[\frac{\kappa(1-\kappa)}{r^2}-\frac{1}{E-V}\frac{\kappa}{r}\frac{dV}{dr}\right]F^{lj}_i(r)=-(E+2M^*-V)(E-V)F^{lj}_i(r), \tag{30}$$

$$\left[\frac{d^2}{dr^2}-\frac{1}{E+2M^*-V}\frac{d(2M^*-V)}{dr}\frac{d}{dr}\right]G^{lj}_i(r)-\left[\frac{\kappa(1+\kappa)}{r^2}+\frac{1}{E+2M^*-V}\frac{\kappa}{r}\frac{d(2M^*-V)}{dr}\right]G^{lj}_i(r)$$
$$=-(E+2M^*-V)(E-V)G^{lj}_i(r), \tag{31}$$

where

$$\kappa(\kappa-1)=l'(l'+1),\quad \kappa(\kappa+1)=l(l+1). \tag{32}$$

It is clear that one can use either Eq. (30) or, equivalently, Eq. (31) to get the eigenvalues E and the corresponding eigenfunctions. Normally Eq. (31) is used in the literature and the spin-orbital splitting is discussed in connection with the corresponding spin-orbital potential

$$\frac{1}{E+2M^*-V}\frac{\kappa}{r}\frac{d(\ 2M^*-V)}{dr}.$$

If Eq. (30) is used instead and the PSOP term

$$\frac{1}{E-V}\frac{\kappa}{r}\frac{dV}{dr}$$

is neglected, then the eigenvalues E for the same l' will degenerate. This is the phenomenon of pseudospin symmetry observed in [1,2]. It means that Eq. (26) is the transformation between the normal spin formalism and the pseudospin formalism.

In Eq. (30), the term which splits the pseudospin partners is simply the PSOP. The hidden symmetry for the pseudospin approximation is revealed as $dV/dr=0$, which is more general and includes $V=0$ discussed in [14] as a special case. For exotic nuclei with highly diffuse potentials, $dV/dr\sim 0$ may be a good approximation and then the pseudospin symmetry will be good. But generally, $dV/dr=0$ is not always satisfied in the nuclei and the pseudospin symmetry is an approximation. However, if

$$\left|\frac{1}{E-V}\frac{\kappa}{r}\frac{dV}{dr}\right|\ll\left|\frac{\kappa(1-\kappa)}{r^2}\right|,$$

the pseudospin approximation will be good. Thus, the comparison of the relative magnitude of the PCB $\kappa(1-\kappa)/r^2$, and the PSOP can provide us with some information on the pseudospin symmetry.

In a recent paper [17], the mechanism behind the pseudospin symmetry was studied and the pseudospin symmetry was shown to be connected to the competition between the PCB and PSOP, which is mainly decided by the derivative of the difference between the scalar and vector potentials. With the scalar and vector potentials derived from a self-consistent RCHB calculation, the pseudospin symmetry and its energy dependence have been discussed. Here in this paper we will extend the previous investigation to the case of exotic nuclei. The pseudospin symmetry for exotic nuclei is investigated for Zr and Sn isotopes from the proton drip line to the neutron drip line. The isospin and energy dependence of the pseudospin approximation will be investigated in detail in the following section.

IV. ENERGY SPLITTING OF THE PSEUDOSPIN PARTNERS

We use here the nonlinear Lagrangian parameter set NLSH [26] which could provide a good description of all nuclei from oxygen to lead. As we study not only the closed shell nuclei, but also the open shell nuclei, the inclusion of pairing is necessary. The pairing interaction strength is the same as in Ref. [22]. The interaction strength in the pairing force of zero range, Eq. (22), is properly renormalized by the calculation of RCHB theory with Gogny force. Since we use a pairing force of zero range, we have to limit the number of continuum levels by a cutoff energy. For each spin-parity channel, 20 radial wave functions are taken into account, which corresponds roughly to a cutoff energy of 120 MeV

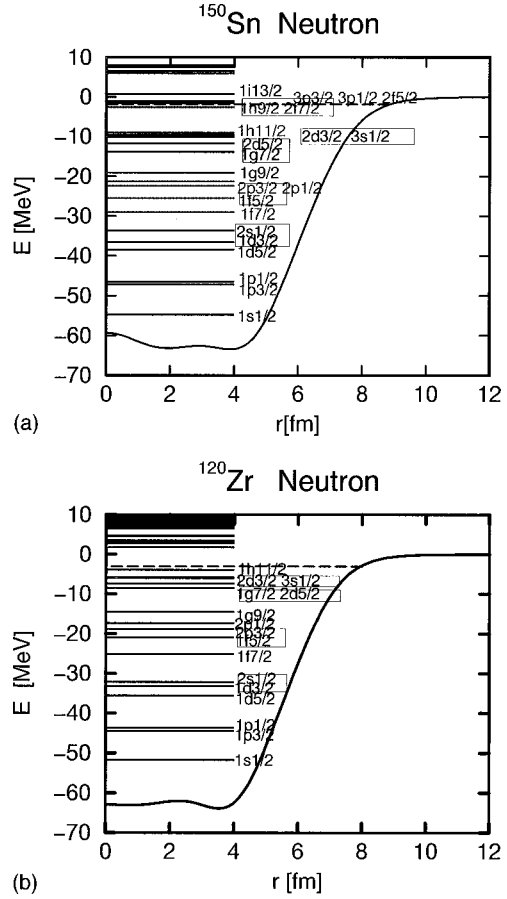

FIG. 1. The single-particle levels in the canonical basis for the neutron in (a) ^{150}Sn and (b) ^{120}Zr. The Fermi surface is shown by a dashed line. The bound pseudospin partners are marked by boxes.

for a fixed box radius $R=20$ fm. For the fixed cutoff energy and for the box radius R, the strength V_0 of the pairing force in Eq. (22) is determined by adjusting the corresponding pairing energy $-\frac{1}{2}\mathrm{Tr}\,\Delta\kappa$ to that of a RCHB calculation using the finite-range part of the Gogny force D1S [25]. We use the nuclear matter density 0.152 fm^{-3} for ρ_0.

The quality of pseudospin symmetry can be understood more clearly by considering the microscopic structure of the wave functions and the single-particle energies in the canonical basis. As shown in Ref. [18], the particle levels for the bound states in a canonical basis are the same as those by solving the Dirac equation with the scalar and vector potentials from RCHB theory. Therefore Eqs. (30) and (31) are valid in the canonical basis after the pairing interaction has been taken into account and are very suitable for a discussion of the pseudospin symmetry.

The neutron single-particle levels in ^{150}Sn and ^{120}Zr are given in Figs. 1(a) and 1(b), respectively. The four sets of pseudospin partners, i.e., $1d_{3/2}$ and $2s_{1/2}$, $1f_{5/2}$ and $2p_{3/2}$, $1g_{7/2}$ and $2d_{5/2}$, and $2d_{3/2}$ and $3s_{1/2}$, are marked by boxes. As seen in the figure, the energy splitting between pseudospin partners decreases with decreasing binding energy. The single-particle energy of $3s_{1/2}$ in ^{120}Zr is -6.00 MeV, and its partner $2d_{3/2}$ is -5.86 MeV; the splitting is 0.14 MeV. While $2s_{1/2}$ is -31.62 MeV, $1d_{3/2}$ -33.23 MeV, the splitting is 1.61 MeV, which is bigger than the former one by a factor of 10. The same situation is found for the energy splitting between pseudospin partners in ^{150}Sn: The single-particle energies of $3s_{1/2}$ and $2d_{3/2}$ are -9.645 and -10.11 MeV, respectively. The single-particle energies for other pseudospin partners in ^{150}Sn are -11.74 and -13.87 MeV for $2d_{5/2}$ and $1g_{7/2}$ partners, -22.46 and -25.50 MeV for $2p_{3/2}$ and $1f_{5/2}$ partners, and -33.63 and -36.58 for $2s_{1/2}$ and $1d_{3/2}$ partners, respectively. Although we show only the neutron single-particle levels in ^{150}Sn and ^{120}Zr as examples here, the same are found in other Sn and Zr isotopes. It is usually seen that the pseudospin symmetry approximation becomes better near the Fermi surface, which is in agreement with the experimental observation.

In Fig. 1 there are also two pairs of pseudospin partners ($3p_{3/2}$ and $2f_{5/2}$ partners and $2f_{7/2}$ and $1h_{9/2}$ partners) near the threshold, apart from the fours pairs of pseudospin partners below the Fermi level. The energies for these two pairs of pseudospin partners are -1.581 and -1.031 MeV for the $3p_{3/2}$ and $2f_{5/2}$ partners and -2.549 and -2.620 MeV for the $2f_{7/2}$ and $1h_{9/2}$ partners, respectively. Considering their pseudospin orbital angular momentum $\tilde{l}=2$ and 4, their splittings

$$\Delta E=\frac{E_{\tilde{l}j=\tilde{l}-1/2}-E_{\tilde{l}j=\tilde{l}+1/2}}{2\tilde{l}+1}$$

are only -0.1100 MeV and 0.7889×10^{-2} MeV, respectively. This is due to the energy dependence and the diffuseness of the potential in exotic nuclei, which we will discuss in the following. The energy dependence of pseudospin partners has been discussed in Refs. [17,14,16]. As is seen in Fig. 1, the normal splitting is such that the orbital $j=\tilde{l}+1/2$ is below the orbital $j=\tilde{l}-1/2$, except for $3p_{3/2}$ and $2f_{5/2}$ partners. The same also happens for $2d_{3/2}$ and $3s_{1/2}$ partners in Zr isotopes. The pseudospin splitting depends on the derivative of the difference between the scalar and vector potentials, dV/dr, which is small for exotic nuclei with a highly diffuse potential. The integration of $(dV/dr)|F|^2$ over r gives the splitting of the pseudospin partners, whose sign will decide the normal splitting or the reverse. The subtle details of the potential are crucial for the pseudospin splitting.

To see the behavior of the pseudospin partners around the Fermi level and the isospin dependence of the pseudospin splitting, we show the single-particle levels near the Fermi surface in the canonical basis for the Sn and Zr isotopes with an even neutron number as a function of the mass number in Fig. 2. The Fermi level is shown by the dashed line. The pseudospin splitting for the pseudospin partners, $2d_{3/2}$ and $3s_{1/2}$, remains small in Zr and Sn isotopes from the proton drip line to the neutron drip line. The pseudospin symmetry remains even valid for exotic nuclei. The pseudospin symmetry near the neutron drip line becomes better than that near the β-stability line. In Fig. 2(a), there is a kink for the single-particle levels in the continuum, as the contribution from the continuum becomes important and the potential becomes diffuse around ^{130}Sn. But the splitting for $3p_{3/2}$ and $2f_{5/2}$ partners and $2f_{7/2}$ and $1h_{9/2}$ partners in Sn isotopes is small and the pseudospin symmetry approximation is very good, independent of whether they are in the continuum or near the threshold. Therefore we can see that pseudospin

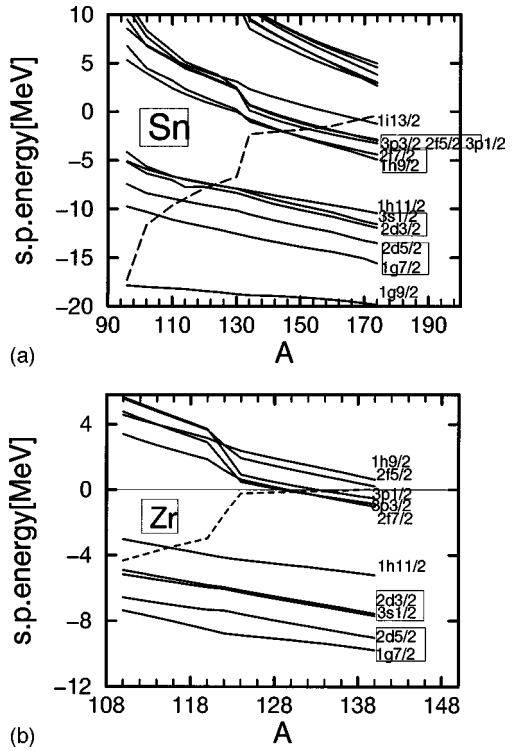

FIG. 2. The single-particle energies of the neutron in the canonical basis as a function of the mass number for (a) Sn and (b) Zr isotopes. The dashed line indicates the chemical potential.

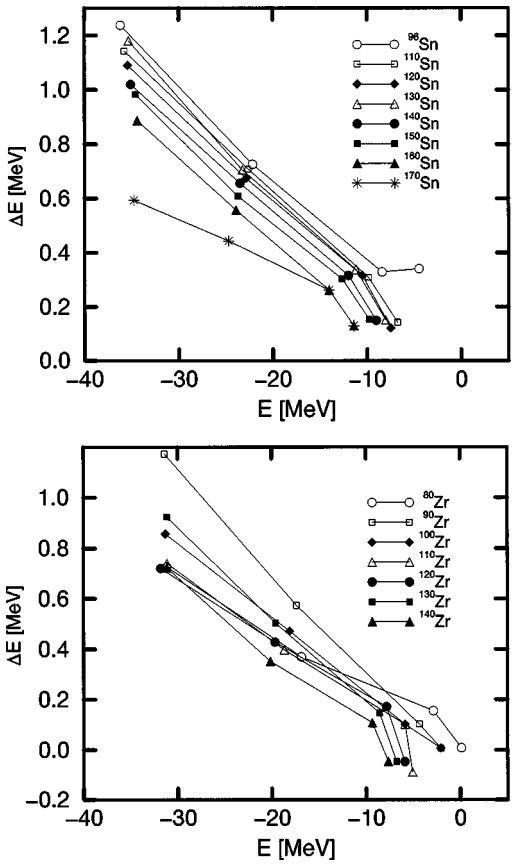

FIG. 3. The pseudospin orbit splitting $\Delta E=(E_{\tilde{l}j=\tilde{l}-1/2}-E_{\tilde{l}j=\tilde{l}+1/2})/(2\tilde{l}+1)$ versus the binding energy $E=[\tilde{l}E_{\tilde{l}j=\tilde{l}+1/2}+(\tilde{l}+1)E_{\tilde{l}j=\tilde{l}-1/2}]/(2\tilde{l}+1)$ for Zr and Sn isotopes. From left to right, the pseudospin partners correspond to $(1d_{3/2},2s_{1/2})$,$(1f_{5/2},2p_{3/2})$,$(1g_{7/2},2d_{5/2})$, and $(2d_{3/2},3s_{1/2})$, respectively.

symmetry is very well preserved for the orbital near the threshod energy and in the continuum region.

In order to see the energy dependence and the isospin dependence of the pseudospin orbital splitting more clearly, we plot

$$\Delta E=\frac{E_{\tilde{l}j=\tilde{l}-1/2}-E_{\tilde{l}j=\tilde{l}+1/2}}{2\tilde{l}+1}$$

versus

$$E=\frac{\tilde{l}E_{\tilde{l}j=\tilde{l}+1/2}+(\tilde{l}+1)E_{\tilde{l}j=\tilde{l}-1/2}}{2\tilde{l}+1}$$

for the bound pseudospin partners in Sn and Zr isotopes in Fig. 3. In both isotopes, a monotonous decreasing behavior with decreasing binding energy is clearly seen. The pseudospin splitting for $3s_{1/2}$ and $2d_{3/2}$ is more than 10 times smaller than that of $2s_{1/2}$ and $1d_{3/2}$. As far as the isospin dependence of the pseudospin orbital splitting is concerned, the splitting in Sn isotopes gives a monotonous decreasing behavior with the increasing isospin. Particularly for $2s_{1/2}$ and $1d_{3/2}$ partners, the pseudospin splitting in ^{170}Sn is only half of that in ^{96}Sn. Just as we expected, the pseudospin symmetry in neutron-rich nuclei is better. In Zr isotopes, although the situation is more complicated (e.g., the effect of the deformation which is neglected here), the pattern is more or less the same, i.e., a monotonous decreasing behavior with decreasing binding energy and a monotonous decreasing behavior with isospin. From these studies, we see that the pseudospin symmetry remains a good approximation for both stable and exotic nuclei. A better pseudospin symmetry can be expected for the orbital near the threshold, particularly for nuclei near the particle drip line.

V. PSEUDOSPIN ORBITAL POTENTIAL

To understand why the energy splitting of the pseudospin partner changes with different binding energies and why the pseudospin approximation is good in RMF energy, the PSOP and PCB should be examined carefully. Unfortunately, it is very hard to compare them clearly, as the PSOP has a singularity at $E\sim V$. As we are only interested in the relative magnitude of the PCB and PSOP, we introduce the effective PCB, $(E-V)\kappa(\kappa-1)/r^2$, and the effective PSOP, $(\kappa/r)dV/dr$, for comparison. They correspond to the PCB and the PSOP multiplied by a common factor $E-V$, respectively.

The effective PSOP does not depend on the binding energy of the single-particle level, but depends on the angular momentum and parity. On the other hand, the effective PCB depends on the energy. Comparing these two effective potentials one can see the energy dependence of the pseudospin symmetry. They are given in Fig. 4 for $s_{1/2}$ (lower) and $d_{3/2}$ (upper) of ^{120}Zr in an arbitrary scale.

The pseudospin approximation is much better for the less bound pseudospin partners, because the effective PCB is

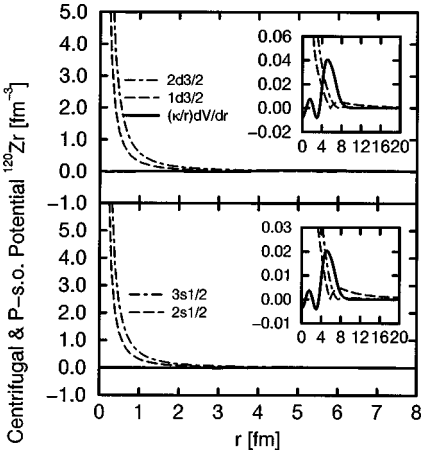

FIG. 4. The comparison of the effective pseudocentrifugal barrier (PCB) $(E-V)\kappa(\kappa-1)/r^2$ (dashed lines and dot-dashed lines) and the effective pseudospin orbital potential (PSOP) $(\kappa/r)dV/dr$ (solid line) in arbitrary scale for $d_{3/2}$ (upper) and $s_{1/2}$ (lower) in ^{120}Zr. The dashed lines are for $1d_{3/2}$ and $2s_{1/2}$, and the dot-dashed lines are for $2d_{3/2}$ and $3s_{1/2}$. The insets show the same quantities, but the ordinate is magnified and the abscissa is reduced to show the behaviors of the effective PCB and the effective PSOP near the nuclear surface.

smaller for the more deeply bound states. This is in agreement with the results shown in Fig. 3. The effective PSOP and the effective PCB are also given as insets in Fig. 4 in order to show their behavior near the nuclear surface.

In order to examine this carefully, we compare the effective PCB (dashed lines or dot-dashed lines) and the effective PSOP (solid lines) multiplied by the squares of the lower component wave function $F(r)$, which are given in Fig. 5, for $2s_{1/2}$ (upper left), $3s_{1/2}$ (lower left), $1d_{3/2}$ (upper right), and $2d_{3/2}$ (lower right) of ^{120}Zr in arbitrary scale. The pseudospin approximation is much better for the less bound pseudospin partners, because the effective PCB is smaller for the more deeply bound states. This is in agreement with the results shown above. The integrated values of the potentials in

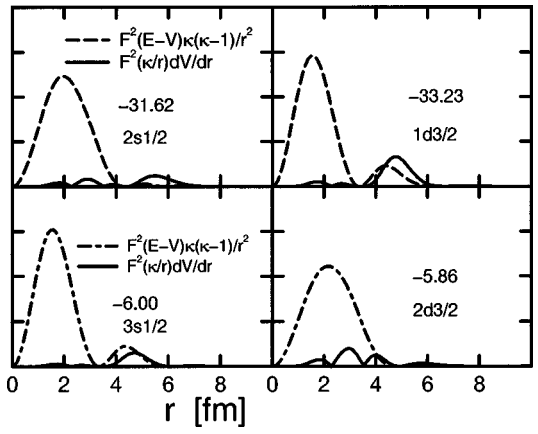

FIG. 5. The comparison of the effective pseudocentrifugal barrier (PCB) $(E-V)\kappa(\kappa-1)/r^2$ (dashed lines and dot-dashed lines) and the effective pseudospin orbital potential (PSOP) $(\kappa/r)dV/dr$ (solid line) multiplied by the square of the wave function F of the lower components in arbitrary scale for $d_{3/2}$ (upper) and $s_{1/2}$ (lower) in ^{120}Zr. The dashed lines are for $1d_{3/2}$ and $2s_{1/2}$, and the dot-dashed lines are for $2d_{3/2}$ and $3s_{1/2}$.

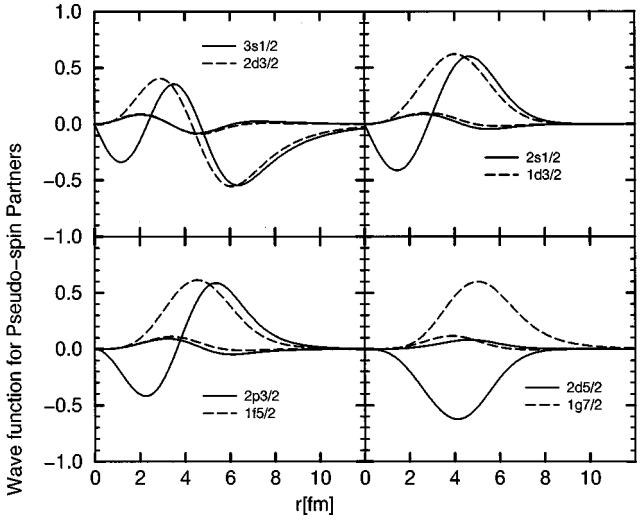

FIG. 6. The upper component G and lower component F of the Dirac wave functions for the pseudospin partners in ^{120}Zr. The phase of the Dirac wave functions for one of the pseudospin partners has been reversed in order to have a careful comparison.

Fig. 2 with r are proportional to their contribution to the energy after some proper renormalization. It is clear that the contribution of the effective PCB (dashed lines or dot-dashed lines) is much bigger than that of the effective PSOP (solid lines). Generally the effective PSOP is two orders of magnitude smaller than the effective PCB.

In Figs. 1 and 2 we notice that the orbital $j=\tilde{l}+1/2$ is generally below the orbital $j=\tilde{l}-1/2$, except for $3p_{3/2}$ and $2f_{5/2}$ partners in Sn isotopes. The same situation also happens for $2d_{3/2}$ and $3s_{1/2}$ partners in Zr isotopes. As the pseudospin splitting depends on the PSOP, which depends on the subtle radial dependence of the potentials, sometimes the PSOP may have positive or negative regions as a function of r which cancel each other. The integration of $(dV/dr)|F|^2$ over r gives the splitting of the pseudospin partners, whose sign will decide the normal splitting or the reverse. That is the reason why the orbital $j=\tilde{l}+1/2$ is above the orbital $j=\tilde{l}-1/2$ for $3p_{3/2}$ and $2f_{5/2}$ partners in Sn isotopes and for $2d_{3/2}$ and $3s_{1/2}$ partners in Zr isotopes.

VI. WAVE FUNCTION OF PSEUDOSPIN PARTNERS

In the above discussion, we have seen that the PSOP is much smaller than the PCB. Therefore, if we neglect the PSOP in Eq. (30), the lower component of the Dirac wave functions for the pseudospin partners will be the same; i.e., in the case of the exact pseudospin symmetry, the lower component of the pseudospin partners should be identical (except for the phase). The upper component of the Dirac wave functions can be obtained from the transformation in Eq. (26), which depends on the quantum number κ. Therefore the study of the Dirac wave functions for the pseudospin partners will provide a check for the pseudospin approximation in nuclei. As examples, the normalized single-nucleon wave functions for the upper (G) and lower (F) components of the Dirac wave functions for the pseudospin partners $1d_{3/2}$ and $2s_{1/2}$, $1f_{5/2}$ and $2p_{3/2}$, $1g_{7/2}$ and $2d_{5/2}$, and $2d_{3/2}$ and $3s_{1/2}$ in ^{120}Zr are given in Fig. 6. Of course, the lower

components are much smaller in magnitude compared with the upper component in Eq. (26). The phase of the Dirac wave functions for one of the pseudospin partners has been reversed in order to have a careful comparison. It is seen that the lower components of the Dirac wave functions for the pseudospin partners are very similar and are almost equal in magnitude, as observed also for ^{208}Pb in Refs. [14,16]. The similarity in the lower components F of the wave function for the pseudospin partners near the Fermi surface is better than for the deeply bound ones. The similarity in the lower components for the pseudospin partners with small pseudospin orbital angular momentum is better than for the ones with large pseudospin orbital angular momentum. As seen in Fig. 6, the similarity for pseudospin partners $2d_{3/2}$ and $3s_{1/2}$ is better than for pseudospin partners $1d_{3/2}$ and $2s_{1/2}$. The similarities for pseudospin partner $2d_{3/2}$ and $3s_{1/2}$, $1d_{3/2}$ and $2s_{1/2}$ are better than for the pseudospin partners $1f_{5/2}$ and $2p_{3/2}$, $1g_{7/2}$ and $2d_{5/2}$.

Although the lower components for the pseudospin partners are very close to each other, the difference for the upper components is very big. The upper component of the Dirac wave functions can be obtained from the transformation in Eq. (26), which for the sperical case can be reduced to the following:

$$G_i^{lj}(r)=\frac{1}{E-V}\left[-\frac{dF_i^{lj}(r)}{dr}+\frac{\kappa}{r}F_i^{lj}(r)\right]. \tag{33}$$

As seen in Fig. 6, in the case of exact pseudospin symmetry, where both E and $F_i^{lj}(r)$ are identical for the pseudospin partners, the upper components $G_i^{lj}(r)$ will be different due to the term $(\kappa/r)F_i^{lj}(r)$. For pseudospin partners with small $\tilde{l}$, the contribution of the term $(\kappa/r)F_i^{lj}(r)$ becomes less important for larger r and a similarity between the upper components can happen in the nuclear surface. As, for example, for $r\geqslant 6$ fm, the upper components for the pseudospin partners $1d_{3/2}$ and $2s_{1/2}$, $1f_{5/2}$ and $2p_{3/2}$, and $2d_{3/2}$ and $3s_{1/2}$ in Fig. 6 are very similar.

VII. SUMMARY

In conclusion, the pseudospin symmetry is examined in normal and exotic nuclei in the framework of RCHB theory. Based on RCHB theory the pseudospin approximation in exotic nuclei is investigated in Zr and Sn isotopes from the proton drip line to the neutron drip line. The quality of the pseudospin approximation is shown to be connected to the competition between the PCB and PSOP, which is mainly decided by the derivative of the difference between the scalar and vector potentials dV/dr. If the derivative of the difference between the scalar and vector potentials dV/dr vanishes, the pseudospin symmetry is exact. The condition $dV/dr\sim 0$ may be a good approximation for exotic nuclei with a highly diffuse potential. Further a new condition

$$\frac{1}{E-V}\frac{\kappa}{r}\frac{dV}{dr}\ll\kappa\frac{(1-\kappa)}{r^2}$$

is found under which the symmetry is preserved approximately. We have examined this condition to see how good the pseudospin symmetry in RCHB theory is. For a given angular momentum and parity channel, the effective PCB, $(E-V)\kappa(\kappa-1)/r^2$, becomes stronger for the less bound level; so the pseudospin symmetry for the weakly bound state is better than that for the deeply bound state, which is in agreement with the experimental observation [1,2]. Pseudospin symmetry is found to be a good approximation even for the exotic nuclei with a highly diffuse potential. The above conclusion has been well supported by RCHB calculations for Zr and Sn isotopes from the proton drip line to the neutron drip line. From the simple Dirac equation, it has been shown that there are two equivalent ways to solve the coupled Dirac equation for the upper and lower components: i.e., the normal spin formalism and pseudospin formalism. Both formalisms are equivalent as far as the energies and wave functions are concerned. Their relation is given by Eq. (26), which indicates that the unitary transformation from the conventional formalism to the pseudospin formalism has ''p helicity'' [12,9,15]. Summarizing our investigation, we conclude the following.

(1) The quality of the pseudospin approximation is connected to the competition between the PCB and PSOP which is mainly proportional to the derivative of the difference between the scalar and vector potentials dV/dr.

(2) The pseudospin symmetry is a good approximation for normal nuclei and becomes much better for exotic nuclei with highly diffuse potentials.

(3) The pseudospin symmetry has a strong energy dependence. The energy splitting between the pseudospin partners is smaller for orbitals near the Fermi surface.

(4) The energy difference between the orbital $j=\tilde{l}+1/2$ and the orbital $j=\tilde{l}-1/2$ is always negative, except for $3p_{3/2}$ and $2f_{5/2}$ partners. The same situation also happens for $2d_{3/2}$ and $3s_{1/2}$ partners in Zr isotopes. The integration of $(dV/dr)|F|^2$ over r gives the splitting of the pseudospin partners, whose sign will decide the normal splitting or the reverse.

(5) The lower components of the Dirac wave functions for the pseudospin partners are very similar and almost equal in magnitude. The similarity in the lower components of the wave function for the pseudospin partners near the Fermi surface is closer than for the deeply bound ones.

ACKNOWLEDGMENT

We would like to express our gratitude to F. L. Pratt for his careful reading of the manuscript.

[1] A. Arima, M. Harvey, and K. Shimizu, Phys. Lett. **30B**, 517 (1969).

[2] K. T. Hecht and A. Adler, Nucl. Phys. **A137**, 129 (1969).

[3] R. D. Ratna Raju, J. P. Draayer, and K. T. Hecht, Nucl. Phys. **A202**, 433 (1973); J. P. Draayer and K. J. Weeks, Ann. Phys. (N.Y.) **156**, 41 (1984).

[4] A. L. Blokhin, T. Beuschel, J. P. Draayer, and C. Bahri, Nucl. Phys. **A612**, 163 (1997); T. Beuschel, A. L. Blokhin, and J. P.

Draayer, *ibid.* **A619**, 119 (1997).
[5] B. Mottelson, Nucl. Phys. **A522**, 1 (1991).
[6] J. Y. Zeng, J. Meng, C. S. Wu, E. G. Zhao, Z. Xing, and X. Q. Chen, Phys. Rev. C **44**, R1745 (1991).
[7] C. Bahri, J. P. Draayer, and S. A. Moszkowski, Phys. Rev. Lett. **68**, 2133 (1992).
[8] O. Castanos, M. Moshinsky, and C. Quesne, Phys. Lett. B **277**, 238 (1992).
[9] A. L. Blokhin, C. Bahri, and J. P. Draayer, J. Phys. A **29**, 2039 (1996).
[10] A. Bohr, I. Hamamoto, and B. R. Mottelson, Phys. Scr. **26**, 267 (1982).
[11] A. B. Balantekin, O. Castaño̱v, and M. Moshinsky, Phys. Lett. B **284**, 1 (1992).
[12] A. L. Blokhin, C. Bahri, and J. P. Draayer, Phys. Rev. Lett. **74**, 4149 (1995).
[13] B. D. Serot and J. D. Walecka, in *The Relativistic Nuclear Many-Body Problem* in *Advances in Nuclear Physics*, edited by J. W. Negele and E. Vogt (Plenum, New York, 1986), Vol. 16.
[14] J. Ginocchio, Phys. Rev. Lett. **78**, 436 (1997).
[15] J. N. Ginocchio and A. Leviatan, Phys. Lett. B **425**, 1 (1998).
[16] J. N. Ginocchio and D. G. Madland, Phys. Rev. C **57**, 1167 (1998).
[17] J. Meng, K. Sugawara-Tanabe, S. Yamaji, P. Ring, and A. Arima, Phys. Rev. C **58**, R628 (1998).
[18] J. Meng, Nucl. Phys. **A635**, 3 (1998).
[19] I. Tanihata, Prog. Part. Nucl. Phys. **35**, 505 (1995).
[20] P. G. Hansen, A. S. Jensen, and B. Jonson, Annu. Rev. Nucl. Part. Sci. **45**, 591 (1995).
[21] J. Meng and P. Ring, Phys. Rev. Lett. **77**, 3963 (1996).
[22] J. Meng and P. Ring, Phys. Rev. Lett. **80**, 460 (1998).
[23] J. Meng, I. Tanihata, and S. Yamaji, Phys. Lett. B **419**, 1 (1998).
[24] J. Boguta and A. R. Bodmer, Nucl. Phys. **A292**, 413 (1977).
[25] J. F. Berger *et al.*, Nucl. Phys. **A428**, 32c (1984).
[26] M. Sharma, M. Nagarajan, and P. Ring, Phys. Lett. B **312**, 377 (1993).